Scientia Iranica D (2014) 21(3), 853–860

Sharif University of Technology
Scientia Iranica
Transactions D: Computer Science & Engineering and Electrical Engineering
www.scientiairanica.com

A wideband twenty-element microwave spatial power combiner

H. Javadi-Bakhsh* and R. Faraji-Dana

Center of Excellence on Applied Electromagnetic Systems, School of Electrical and Computer Engineering, College of Engineering, University of Tehran, Tehran, P.O. Box 14395-515, Iran.

Received 30 July 2012; received in revised form 19 April 2013; accepted 15 October 2013

KEYWORDS
Spatial power combiner;
Wideband;
Coaxial structure;
Antipodal finline;
Optimum taper.

Abstract. In this paper, a wideband coaxial power combiner with tray configuration, employing twenty 1-Watt elements mounted on antipodal finline boards, is implemented to achieve a rather high power microwave amplifier in the frequency band of 6-18 GHz. The average gain, Continuous Wave (CW) output power and Power-Added Efficiency (PAE) of the combiner are measured as 17 dB, 15 Watts and 17%, respectively with ripples of less than 3 dB. In order to investigate the combining efficiency, the passive structure is fabricated and tested in the first step. Its main components, i.e. the coaxial adapter and the antipodal finline boards, are synthesized by using Klopfenstein's optimum impedance taper, and simulated by Ansoft HFSS. Next, the active devices are added to the system. Stability, thermal management and life time issues are examined and addressed in this step. The system reliability is also demonstrated as graceful degradation due to the failure of devices.

1. Introduction

Coherent power combining platforms of high performance solid-state Monolithic Microwave Integrated Circuits (MMICs) can be an alternative to the Traveling Wave Tube Amplifiers (TWTA) in wireless communication, radar and remote sensing applications. Due to the increasing loss of corporate schemes in the large scale combiners, spatial power combining techniques have noticeably evolved, particularly over the last two decades [1,2]. These techniques are expected to improve the combined output power of a large quantity of amplifiers to a level contending with TWTAs.

Among the diverse proposed structures, the waveguide-based tray-approach [3,6] has demonstrated remarkable power-bandwidth characteristics in the microwave band. Because of the TEM mode of propagation and the symmetry involved, the coaxial waveguide structures employing antipodal finline trays are shown to be most suitable as the ultra-broadband low-loss and low-dispersive configurations compatible with the MMICs [7,8]. Although probe-based conical [9] and radial [10] structures have also been proposed to form a rather wideband combiner with simpler and more affordable building, the coaxial structure seems to be unrivaled in multi-octave applications. Figure 1(a) depicts the overall coaxial combiner whose passive structure is composed of two main parts: the coaxial adapter and the antipodal finline array.

In this paper, the design procedure, implementation and measurement results of a twenty-element combiner over a frequency band of 6 to 18 GHz, is presented. The adapter and the antipodal finline are synthesized using Klopfenstein's optimum impedance taper, based on the small reflection theory [11,12]. In Section 2, the design procedure for the passive structure is presented along with the experimental

*. *Corresponding author. Tel.: +98 21 82084206; Fax: +98 21 88335268*
E-mail addresses: h.javadibakhsh@ut.ac.ir (H. Javadi-Bakhsh); reza@ut.ac.ir (R. Faraji-Dana)

results of the fabricated system. Section 3 gives an overview of the active combiner and the relevant discussions about its stability, graceful degradation, thermal management and life time. Some concluding remarks are given in Section 4.

2. Passive structure

2.1. Structure assembly

Twenty identical wedge-shape trays have been stacked together around an axial post, forming an oversized coaxial waveguide to confine the electromagnetic field. Carried by each tray is an 8 mil RO4003 PCB, which includes a tapered antipodal finline integrated with a finline-to-microstrip balun (Figure 1(b)). It is clear that, as the fins come together, the radial electric field at one end rotates by 90 degrees to become compatible with the microstrip line at the other end [13]. At both ends of the oversized waveguide, a coaxial adapter provides a smooth transition to a standard 50 Ω SMA connector. To this end, the interior conductor of the transition is made of a conical conductor with its one end connected to the inner conductor of the waveguide and the other end to a pin that is the center conductor of a standard 50 Ω SMA connector. The exterior conductor of the transition is a cap connected to the outer conductor of the waveguide and narrowing linearly to the flange section of the SMA connector. The open structure of the assembled combiner is shown in Figure 2(a).

2.2. Design

Some issues must be considered in selecting the radii of the waveguide. If a larger dimension is chosen, the complicated higher-order modes of the structure become stronger. This will lead to less accurate modeling and loss of combining efficiency. For smaller dimensions, however, one should be concerned with the accommodation of the boards inside the waveguide, the machining of the trays and the thermal management of the structure. Considering these facts, the radii of the waveguide are selected to be 10 mm and 16.5 mm. The characteristic impedance, Z_0 (in Ω), of an air-filled coaxial waveguide with inner and outer radii of a and b, respectively, is given by [12]:

$$Z_0 \approx 60 \ln(\frac{b}{a})[\Omega]. \quad (1)$$

So, the characteristic impedance at the over-sized waveguide is 30 Ω. Therefore, the transition adapter should transform the 50 Ω impedance of the connector to 30 Ω. This, in turn, implies that in the 20-element combiner, an impedance of 600 Ω, which is 30 Ω multiplied by 20, should be matched to the standard 50 Ω of an MMIC by the antipodal finline board. This is illustrated in Figure 3(a). To minimize the length, thus reducing the loss of combiner, we use the optimum transmission-line impedance taper to synthesize the cone and the antipodal finline, as derived in [14] for the case of a rectangular waveguide packaging. Figure 3(b) shows a tapered transmission-

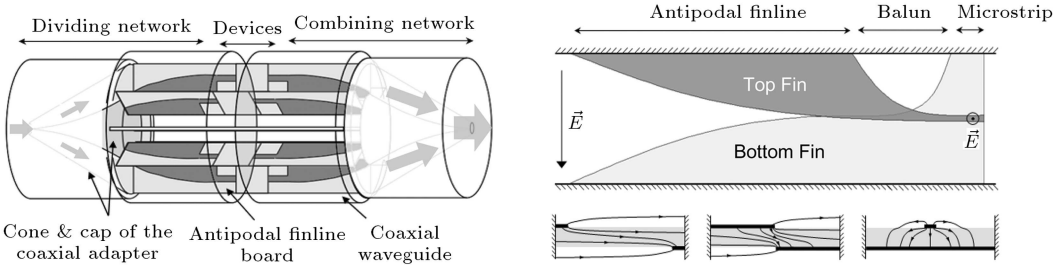

Figure 1. (a) Ultra-wideband coaxial spatial power combiner. (b) Electric field rotation by 90 degrees in the antipodal finline to microstrip.

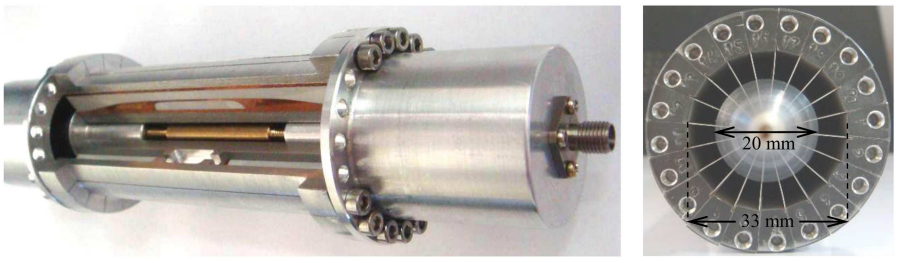

Figure 2. (a) Assembled passive structure (with some trays removed). (b) Cross-section view of the oversized coaxial waveguide.

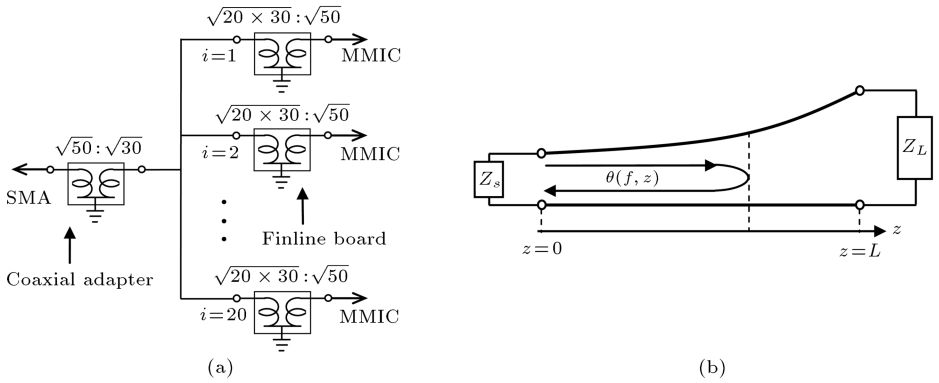

Figure 3. (a) Impedance matching equivalent circuit at the oversized waveguide opening. (b) The tapered transmission-line model to transform impedances.

line transforming the load Z_L to the source Z_S at the input with the characteristic impedance $Z(z)$ and phase constant $\beta(f,z)$, where z and f are the positions along the taper and the frequency, respectively. In order to keep the input reflection coefficient below a desired value of Γ_m on the frequency band, larger than the cutoff frequency, f_0, i.e. $\Gamma_{in}(f \geq f_0) \leq \Gamma_m$, $Z(\theta)$ must take the following form in an optimum taper [11,12]:

$$\ln\left(\frac{Z(\theta)}{Z_0}\right) = \frac{1}{2}\ln\left(\frac{Z_L}{Z_0}\right) + \Gamma_m A^2 \int_0^{\chi} \frac{I_1(A\sqrt{1-y^2})}{A\sqrt{1-y^2}}dy, \qquad (2)$$

where:

$$A = \cos h^{-1}\left(\frac{\Gamma_0}{\Gamma_m}\right),$$

$$\Gamma_0 = \frac{1}{2}\ln\left(\frac{Z_L}{Z_S}\right),$$

$$\theta = \theta(f,z) = 2\int_0^z \beta(f,z')dz',$$

$$\chi = \frac{2\theta}{\theta_t} - 1,$$

$$\theta_t = \theta|_{z=L},$$

and $I_1(x)$ is the first order modified Bessel function. Considering the monotonically increasing phase constant, $\beta(f,z)$, the following condition must be satisfied at the lowest frequency, f_0:

$$\theta_t(f_0) \geq 2A, \qquad (3)$$

which implicates the inverse proportionality of the minimum length of the taper to f_0 and Γ_m.

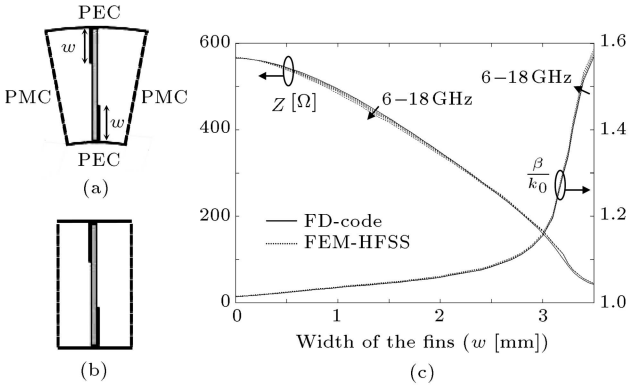

Figure 4. (a) Sectoral waveguide cell modeled with PEC and PMC walls analyzed by HFSS. (b) Approximately rectangular cell of (a) analyzed by finite difference (FD) method. (c) Characteristic impedance and normalized phase constant versus the fin width for the cells of (a) and (b).

2.3. Synthesis

The phase constant of TEM-mode in the adapter is almost equal to the free-space wave number, k_0, independent of the position, z. The situation is obviously different in the finlines, where the phase constant is dependent on the width of the fins. The cross section of the oversized waveguide loaded with finlines is shown in Figure 2(b). Here, the electrical contact of fins with the waveguide is assumed to be perfect. Due to the symmetric loading and negligible higher-order modes, the analysis zone can be reduced to just one sectorial waveguide cell, whose boundaries are PEC and PMC, as shown in Figure 4(a).

This cell is easily analyzed by HFSS at frequencies 6, 10, 14 and 18 GHz to acquire phase constant and characteristic impedance with respect to the fin width. This cell can be approximated with a rectangular cell, as shown in Figure 4(b), which is normally analyzed by the spectral domain method [14,15]. In our synthesis, however, we employed the much simpler Finite Difference (FD) method to analyze this cell. Figure 4(c) compares the results of HFSS and the

FD code generated for this purpose. Excellent agreements are observed. It is seen that the characteristic impedance decreases, while the normalized phase constant increases as the fin width increases. No significant effects are observed by changing the frequency. It may be noted that due to the dielectric loading in the cell, the impedance at $w = 0$ is lower than the expected 600 Ω.

To find $w(z)$ from the computed values of $Z(w)$ and $\beta(w)$, which determines the shape of the antipodal finlines, one may use the algorithm of Figure 5. In this algorithm, the length of taper, L, is divided into N segments of length, $\Delta z = L/N$, to approximate θ by:

$$\theta(z_i) \approx 2\sum_{k=0}^{i-1} \beta(z_k)\Delta z = \theta(z_{i-1}) + 2\beta(z_{i-1})\Delta z, \quad (4)$$

where $z_i = i\Delta z$ for $i = 1, 2, ..., N$. By setting the total round-trip phase to an initial value, like $\theta_t^0 = 2L\bar{\beta}$ in which $\bar{\beta}$ is the mean value of $\beta(w)$, $Z(\theta)$ can be found by Eq. (2). By using a recursive calculation, i.e. $\beta(z_i) \rightarrow \theta(z_{i+1}) \rightarrow Z(z_{i+1}) \rightarrow w(z_{i+1}) \rightarrow \beta(z_{i+1})$, one can evaluate all subsequent values, starting from the initial condition θ, $w = 0$ at $z = 0$. The procedure is iterated by the updated $\theta_t = \theta(z_{i=N})$ until θ_t converges. Then, Condition (3) is verified, which determines whether L should be increased. Ultimately, smooth converged $w(z)$ is concluded by increasing N to an adequately large number.

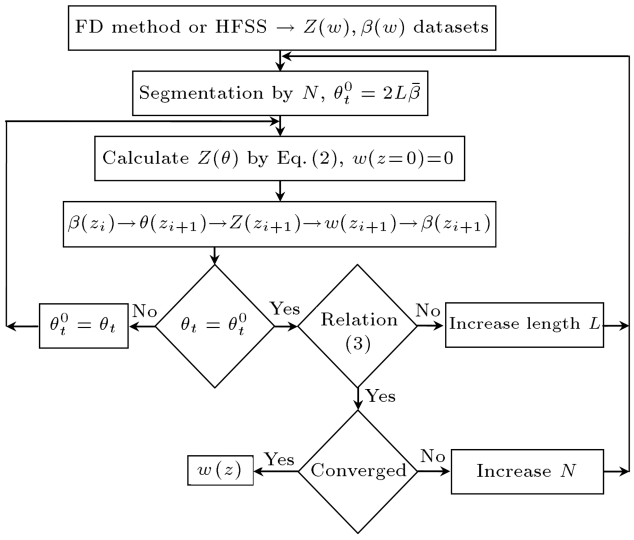

Figure 5. Algorithm for synthesizing of the antipodal finline.

Figure 6 shows the shape of the transition adapter and the finlines computed by the above-mentioned algorithm.

2.4. Simulation and measurement

Using symmetry, one may just consider $\frac{1}{20}$ of the passive structure as a model to simulate its performance using HFSS. Assuming that the balun is free of any in-band resonances, the transitions at both layers are shaped exponentially with some tuning to improve the frequency response over the desired band. Figure 7(a) compares the simulated $|S_{11}|$ and $|S_{21}|$ with the measured values of the fabricated structure. Acceptable agreements are observed. It is seen that $|S_{11}|$ is better than 10 dB in the 6 to 18 GHz frequency band, and $|S_{21}|$ is about -2 dB, with some resonances beyond 22 GHz. The observed discrepancies can be mainly attributed to the imperfect modeling, fabrication tolerances, connector losses and measurement errors. The group delay is also shown in Figure 7(b). It is observed that it is flat over the desired frequency band, as required for a low-dispersive broadband structure.

The dissipative loss of the combining network, which is identical to the dividing network, and known as the Power Combining Efficiency (PCE), can be approximated by one half of the loss of the whole structure; so, it can be calculated by [14]:

$$\text{PCE} \approx \frac{|S_{21}|}{\sqrt{1-|S_{11}|^2}}, \quad (5)$$

where $|S_{11}|$ and $|S_{21}|$ are the scattering parameters of the passive structure. Using the results of Figure 7(a), the power combining efficiency of the structure is estimated to be about 80-90 percent.

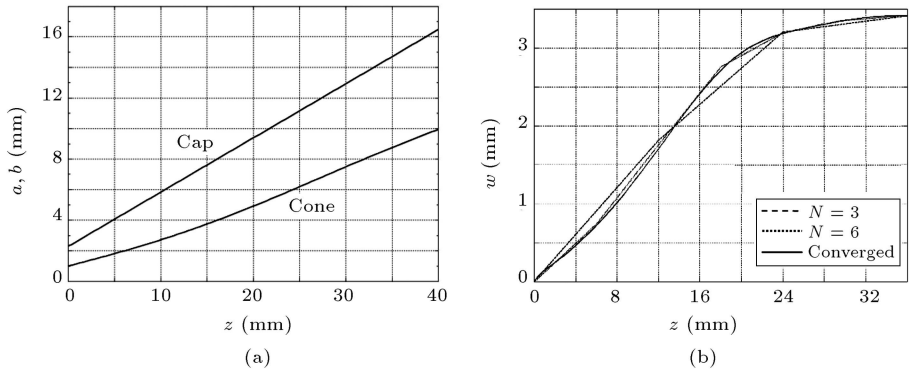

Figure 6. Synthesized shape of the passive structure: (a) Radii of coaxial adapter; and (b) width of the antipodal finline.

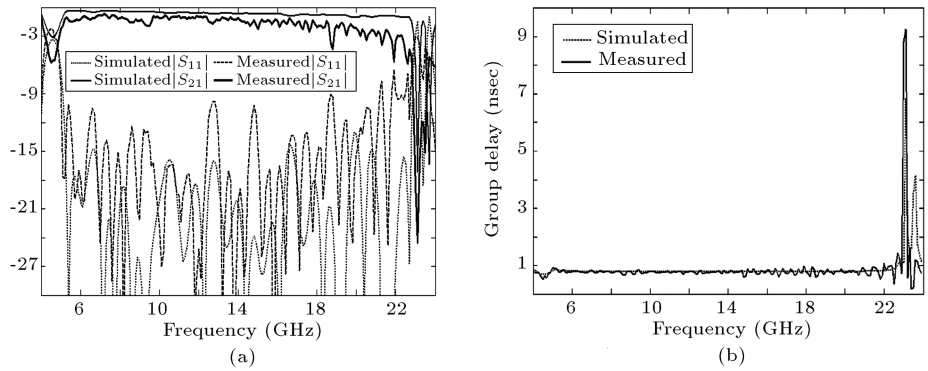

Figure 7. Simulated and measured frequency response of the passive structure: (a) Scattering parameters; and (b) group delay.

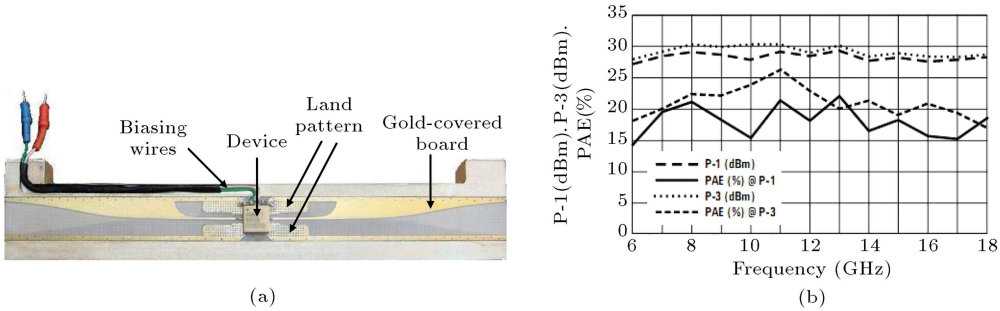

Figure 8. (a) Assembly of active tray. (b) Output power and PAE specification of the device from the vendor datasheet [16].

3. Active combiner

3.1. Fabrication and measurement

The fabricated structure is shown in Figure 2. Figure 8(a) shows a tray on which the gold-plated copper finline board is located. Gold-plating is vital to avoid copper oxidation. The AMMP-6408 SMT packaged MMIC amplifier [16] has been used as the active device (Figure 8(b)). The device is soldered on a land pattern recommended for its proper heat conduction. The device works over a 6-18 GHz frequency band, with average gain and P-1 of 18 dB and 29 dBm, respectively. The average return losses of the device are given as 3 and 9 dB at input and output, respectively, that is a poor matching to 50 Ω, which is normal for wideband amplifiers. The device package provides easy assembly on a microstrip structure and it offers biasing connections on one side. It also needs an around −1 V line at the gate to adjust the drain current to 650 mA supplied by a +5 V line. The embedded wires inside the carrier are to bias the package. Also, ac-bypassing capacitors are located as near as possible to the bias leads.

Figure 9 shows the measured small-signal scattering parameters of the power combiner compared to the simulated results, which are obtained by the Agilent ADS. To do this, a cell (i.e. 1/20) of the combining network, shown in Figure 9(a), is simulated by HFSS and the results are imported to ADS as S2P file with a back to back arrangement, as shown in Figure 9(b). It is then combined with a two-port block of an amplifier given with a S2P file provided by the vendor [16]. It is observed that the gain of the combiner is about 17 dB with ripples of less than 3 dB, and the backward isolation is better than −40 dB. The poor return loss is anticipated due to the device specifications mentioned before. The observed discrepancy between the measured and simulated gain of the combiner can mainly be attributed to gain degradation, due to the temperature increase in the structure, and the imperfect combining, due to the existing variations between the devices.

Figure 10 shows a picture of the fabricated power combiner in the power measurement setup, with its biasing network consisting of twenty separate supply units to bias the devices independently. The structure was fed by another AMMP-6408 as a driver of the combiner to boost the individual twenty devices to saturated power operation. The measured output power and power-added efficiency of the combiner compared with the expected values are given in Figure 11(a). It is obvious that the combiner can be rated as a 15 Watt output power and 17% PAE power amplifier in the frequency range of 6 to 18 GHz. The expected values are computed using the device values given in its datasheet (Figure 8(b)), and the dissipated power loss measured in the passive structure. To justify the higher measured values at some points, compared to

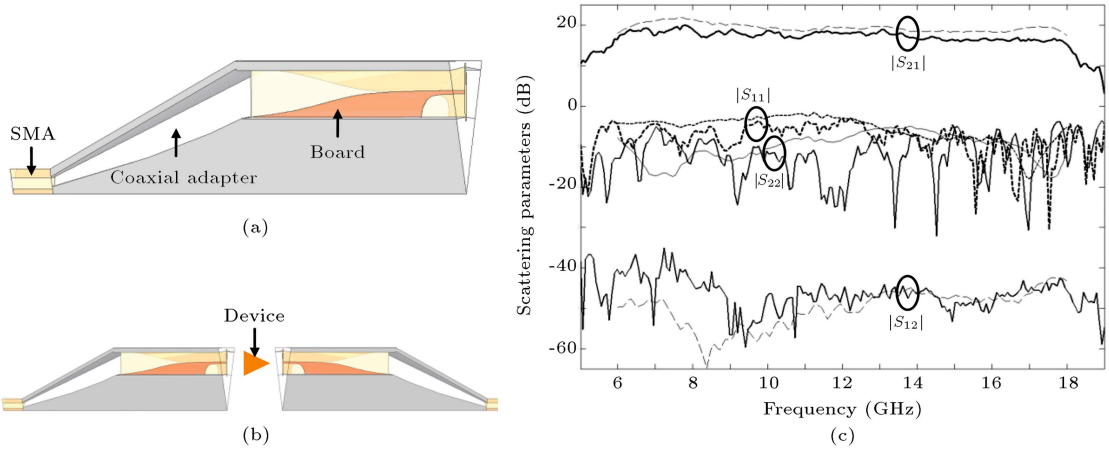

Figure 9. (a) A cell (i.e. 1/20) of the dividing/combining network in HFSS. (b) Back-to-back simulation in ADS. (c) Small-signal scattering parameters (in each pair, the narrow and the wide lines are from simulation and measurements, respectively).

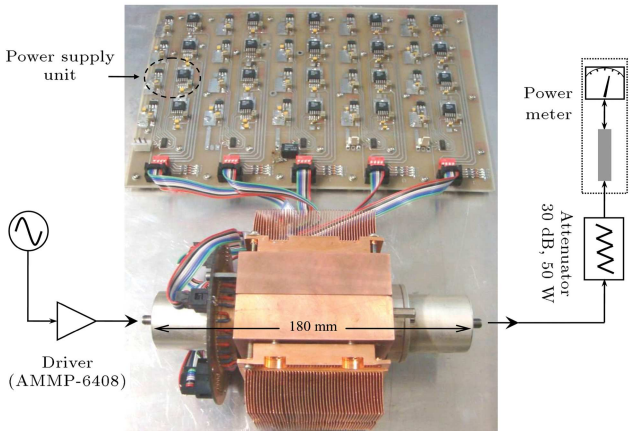

Figure 10. The power combiner with heat-sink and biasing network in measurement setup.

the expected values, one may note that the device performance reported in its datasheet (Figure 8(b)) is lower than that achieved in a practical circuit, due to the unexpected losses in the measurement fixture setup.

3.2. Graceful degradation

In a combiner, conventional experiments have shown that the output degrades gracefully as the devices fail. It has been shown that in a well-matched combining network with independent identical devices, the normalized failed output power can be written as [17]:

$$\frac{P_f}{P_o} = (1 - \frac{m}{N})^2, \tag{6}$$

where m and N are the number of failed devices, and the total number of devices, respectively. Figure 11(b) depicts the normalized failed power of the combiner measured at 8, 12 and 16 GHz compared to Eq. (6). It is observed that the measured values agree well with Relation (6), which shows the graceful degradation of the system.

3.3. Stability

Although the system is expected to be unconditionally stable, a high-gain device fed back by any unpredicted mode in a complicated waveguide medium makes it susceptible to oscillation. However, in our system,

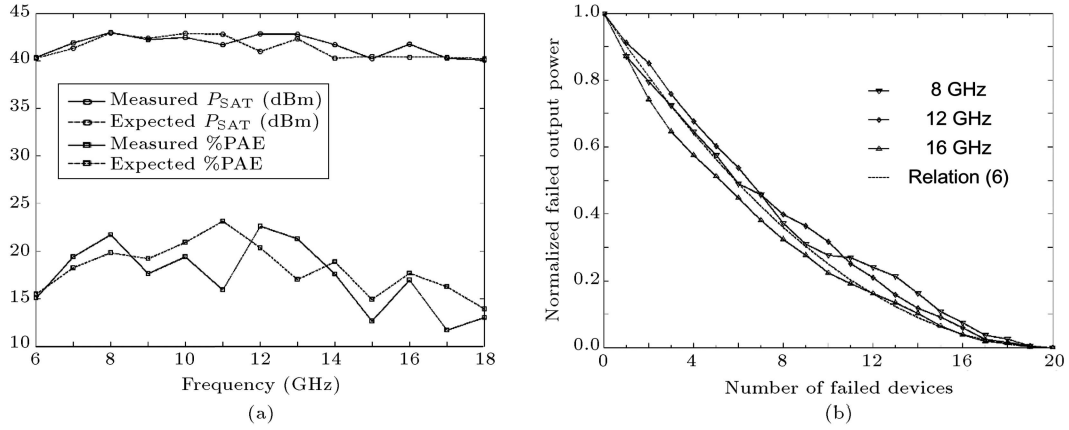

Figure 11. (a) Output power and PAE% of the combiner at saturation. (b) Graceful degradation of output power as devices fail.

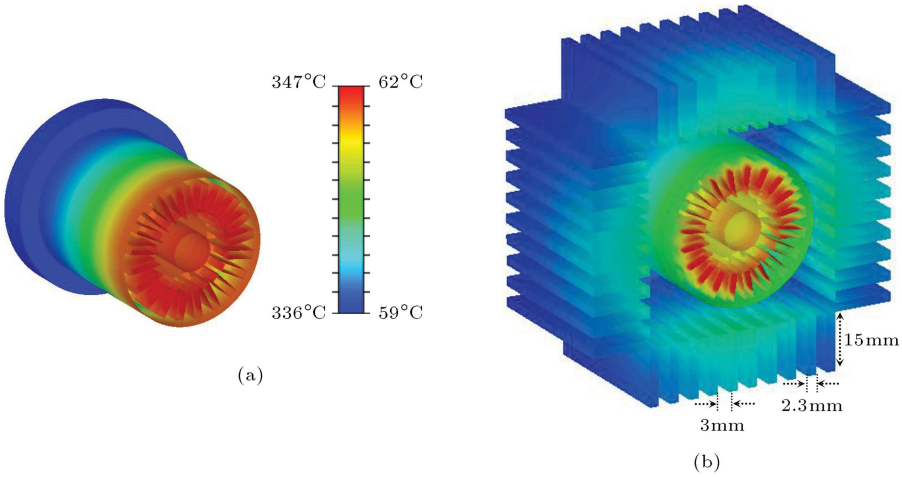

Figure 12. Simulation of the temperature distribution on the structure (a) without a heat-sink, and (b) with a heat-sink.

the moderate gain of the amplifier and the isolation between the input and output ports prevented any undesired oscillations in the whole frequency band. Nevertheless, the trays' housing is large enough to accommodate absorbers if required. With no input RF, we examined the output of the combiner on a spectrum analyzer. Our observations show that slack contacts between the trays and even slight deviation from the axial symmetry of the structure in the assembly process can cause occasional oscillations.

3.4. Thermal management and life time

Wideband amplifiers near to class A have low drain efficiency, typically below 30%, leading to abundant heat dissipation, which should be managed properly. Figure 12 shows that a simple aluminum heat sink can reduce the temperature of the combiner to as low as 60°C. The thermal simulation has been carried out by CST MPhysics Studio software. Specified by the vendor, the thermal resistance of the AMMP-6408 device mounted on a resembling board is about 20°C/Watt [16]; so, the channel of the 3.25 Watt devices installed in the combiner with the above-mentioned heat sink will have a temperature of $(3.25 \times 20 + 60)°C = 125°C$. Therefore, using the mean time between failures data of the device [16], a life time of around 30 years is expected, which is at least twice that of a TWT.

4. Conclusion

A wide-band spatial power combiner using a coaxial waveguide was presented in this paper. It consists of twenty trays placed uniformly around the perimeter of an over-sized coaxial waveguide. Each tray contains an antipodal finline board connected to a MMIC amplifier. Using one-watt MMIC devices, the average output power and the power-added efficiency of 15 Watts and 17%, with a ripple of 3 dB over 6-18 GHz, respectively, were achieved. Good stability inherent with the structure, possible thermal management and reliability are among the main advantages of the designed combiner.

References

1. Delisio, M.P. and York, R.A. "Quasi-optical and spatial power combining", *IEEE Trans. Microwave Theory Tech.*, **50**(3), pp. 929-936 (2002).
2. Bialkowski, M.E. and Tsai, F.E. "Power combiners and dividers", In *Encyclopedia of RF and Microwave Engineering*, K. Chang, Ed., John Wiley & Sons Inc., pp. 3869-3891, Hoboken, New Jersey (2005).
3. Cheng, N.S., Alexanian, A., Case, M.G., Rensch, D.B. and York, R.A. "40 watt CW broadband spatial power combiner using dense finline arrays", *IEEE Trans. Microwave Theory Tech.*, **47**(7), pp. 1070-1076 (1999).
4. Cheng, N.S., Jia, P., Rensch, D.B. and York, R.A. "A 120-W X-band spatially combined solid-state amplifier", *IEEE Trans. Microwave Theory Tech.*, **47**(12), pp. 2557-2561 (1999).
5. Jia, P., Chen, L.Y. and York, R.A. "Multi-octave spatial power combining in oversized coaxial waveguide", *IEEE Trans. Microwave Theory Tech.*, **50**(5), pp. 1355-1360 (2002).
6. Jia, P., Chen, L.Y. and York, R.A. "Broadband high power amplifier using spatial power combining technique", *IEEE Trans. Microwave Theory Tech.*, **51**(12), pp. 2469-2475 (2003).
7. Jia, P. "Broadband power combining device using antipodal finline structure", Capwireless Inc., U.S. Patent 7215220, 5/2007.
8. Jia, P. "A 2 to 20 GHz high power amplifier using spatial power combining techniques", *Microwave Journal*, **48**(4) (April 2005).
9. de Villiers, D.I.L., van der Walt, P.W. and Meyer, P. "Design of conical transmission line power combiners using tapered line matching sections", *IEEE Trans. Microwave Theory Tech.*, **56**(6), pp. 1478-1484 (2008).

10. Song, K., Fan, Y. and He, Z. "Broadband radial waveguide spatial combiner", *IEEE Microwave and Wireless Component Letters*, **18**(2), pp. 73-75 (2008).
11. Klopfenstein, R.W. "A transmission-line taper of improved design," *Proc. of the IRE*, **44**(1), pp. 31-35 (1956).
12. Pozar, D.M., *Microwave Engineering*, 3rd Ed., John Wiley & Sons Inc., New York (2005).
13. Jeong, J., Kwon, Y., Lee, S., Cheon, C. and Sovero, E.A. "1.6- and 3.3- W power amplifier modules at 24 GHz using waveguide-based power-combining structures", *IEEE Trans. Microwave Theory Tech.*, **48**(12), pp. 2700-2708 (2000).
14. Jia, P., Chen, L.Y., Cheng, N.S. and York, R.A. "Design of waveguide finline arrays for spatial power combining", *IEEE Trans. Microwave Theory Tech.*, **49**(4), pp. 609-614 (2001).
15. Hosseini, S.E. and Banai, A. "Ultrabroadband power amplifier using 16-way spatial combining finline array", *Wiley Microwave and Optical Technology Letters*, **55**(2), pp. 454-460 (2013).
16. http://www.avagotech.com
17. Rutledge, D.B., Cheng, N.S., York, R.A., Weikle, R.M. and DeLisio, M.P. "Failures in power combining arrays", *IEEE Trans. Microwave Theory Tech.*, **47**(7), pp. 1077-1082 (1999).

Biographies

Hadi Javadi-Bakhsh received his BS (ranked first) and MS degrees in Electrical Engineering from Iran University of Science and Technology and the University of Tehran, Tehran, Iran, in 2003 and 2011, respectively. From 2006 to 2008, he worked on the design and implementation of ultra-wideband front-end receivers, and, in his MS thesis, he worked on the design, simulation and fabrication of broadband microwave spatial power combining structures. His research interests include large-scale power combiners, design and optimization of passive and active circuits, especially power amplifiers.

Reza Faraji-Dana received a BS degree (honors) from the University of Tehran, Iran, in 1986, and MS and PhD degrees from the University of Waterloo, ON, Canada, in 1989 and 1993, respectively, all in Electrical Engineering. He was a Postdoctoral Fellow with the University of Waterloo for one year, and is currently Professor in the School of Electrical and Computer Engineering at the University of Tehran, Iran, where he was Dean of the Faculty of Engineering for more than four years. He was President of Tehran University until December 2005, Chairman of the IEEE-Iran Section from 2007 till 2009, and is presently Associate member of Iran Academy of Sciences.

He is author and/or coauthor of over 120 technical papers published in reputable international journals and refereed conference proceedings. He received the Institution of Electrical Engineers Marconi Premium Award in 1995 and two national awards in 2010 and 2012. He has been on sabbatical leave with the University of Waterloo since September 2012.